

# Assessment of Critical Stack Pressure and Temperature in Li-Garnet Batteries

Matthias Klimpel, Huanyu Zhang, Giulia Paggiaro, Romain Dubey, Faruk Okur, Lars P.H. Jeurgens, Kostiantyn V. Kravchyk,\* and Maksym V. Kovalenko\*

Stack pressure and temperature serve as effective means to induce deformation of the lithium metal anode toward the Li/solid-state-electrolyte interface, thereby mitigating the well-known issue of void formation during high-current-density stripping. In this study, a compelling methodology is systematically assessed for determining the critical stack pressure and temperature of Li metal anode in conjunction with  $\text{Li}_7\text{La}_3\text{Zr}_2\text{O}_{12}$  (LLZO) solid-state electrolyte, which is the minimum set of values required to maintain conformal contact between Li and LLZO at a given current density. The methodology is based on the analysis of the second derivatives of the voltage profiles of identical Li/LLZO/Li symmetric cells measured during one half-cycle ( $3 \text{ mAh cm}^{-2}$ ) at the same current density but different stack pressures. The effectiveness of the presented approach in assessing conditions for mitigating void formation during Li stripping is evaluated through cycle stability tests performed on Li/LLZO/Li symmetric cells.

play a pivotal role in enabling the use of a lithium metal anode.<sup>[1]</sup> Amid the myriad of candidates in the realm of “solid-state electrolytes”,<sup>[2]</sup>  $\text{Li}_7\text{La}_3\text{Zr}_2\text{O}_{12}$  (LLZO) with garnet-type structure has attracted significant attention in recent years due to its compelling set of properties.<sup>[3,4]</sup> These include high Li-ion conductivity (reaching up to  $1 \text{ mS cm}^{-1}$  at room temperature),<sup>[5,6]</sup> low electronic conductivity ( $\approx 10^{-8} \text{ S cm}^{-1}$  at room temperature),<sup>[7]</sup> exceptional thermal stability,<sup>[8]</sup> and compatibility with metallic Li.<sup>[9–11]</sup> However, as of now, Li-garnet solid-state batteries (SSB) have not met the requirements for commercial viability.<sup>[12–14]</sup> One of the most substantial challenges associated with employing metallic Li in conjunction with LLZO solid-state electrolyte is the appearance of

Kirkendall voids at the Li/LLZO interface during Li stripping.<sup>[15]</sup> As described by Janek et al.,<sup>[16]</sup> these voids form due to an insufficient rate of mass transport, arising from low Li diffusion and applied pressure, which hinders the replenishment of Li that dissolves into the solid electrolyte. As a result, this phenomenon leads to a reduction in the Li/LLZO contact area and a subsequent rise in local current densities, also known as current focusing effect, at the Li/LLZO interface during the subsequent Li plating.<sup>[15–18]</sup> The emergence of voids can, in turn, initiate the growth of Li dendrites at significantly lower current densities than those necessary for dendrite formation in an unstripped Li/LLZO interface.

Since void formation during Li stripping is significantly influenced by the external operating conditions, in particular the stack pressure applied to the cell, their effect on the Li/LLZO interface was recently investigated.<sup>[19–22]</sup> Namely, Sakamoto et al.<sup>[19]</sup> in his pioneering study aimed to determine the critical stack pressure, which represents the minimum pressure required for electrochemical Li stripping without the occurrence of voids at the Li/LLZO interface. The proposed methodology involved monitoring the overpotential of Li/LLZO/Li symmetrical cells under a constant applied current density (ranging from  $0.005$  to  $0.4 \text{ mA cm}^{-2}$ ) while the stack pressure was gradually reduced from  $3.5 \text{ MPa}$  to  $1 \text{ MPa}$  in  $0.5 \text{ MPa}$  steps. The critical stack pressure for a given current density was identified as the point at which a significant increase in overpotential was observed. For instance, it was determined that at a current density of  $0.2 \text{ mA cm}^{-2}$ , the critical stack pressure was

## 1. Introduction

The pursuit of high-energy-density Li-ion batteries has sparked a surge of research into various solid-state electrolytes, which

M. Klimpel, H. Zhang, G. Paggiaro, R. Dubey, F. Okur, K. V. Kravchyk, M. V. Kovalenko

Laboratory of Inorganic Chemistry  
Department of Chemistry and Applied Biosciences  
ETH Zürich

Zürich CH-8093, Switzerland

E-mail: [kravchyk@inorg.chem.ethz.ch](mailto:kravchyk@inorg.chem.ethz.ch); [mvkovalenko@ethz.ch](mailto:mvkovalenko@ethz.ch)

M. Klimpel, H. Zhang, G. Paggiaro, R. Dubey, F. Okur, K. V. Kravchyk, M. V. Kovalenko

Laboratory for Thin Films and Photovoltaics

Empa

Swiss Federal Laboratories for Materials Science & Technology  
Dübendorf CH-8600, Switzerland

L. P. Jeurgens

Laboratory for Joining Technologies & Corrosion

Empa – Swiss Federal Laboratories for Materials Science & Technology  
Dübendorf CH-8600, Switzerland

 The ORCID identification number(s) for the author(s) of this article can be found under <https://doi.org/10.1002/admi.202300948>

© 2024 The Authors. Advanced Materials Interfaces published by Wiley-VCH GmbH. This is an open access article under the terms of the [Creative Commons Attribution](#) License, which permits use, distribution and reproduction in any medium, provided the original work is properly cited.

DOI: 10.1002/admi.202300948

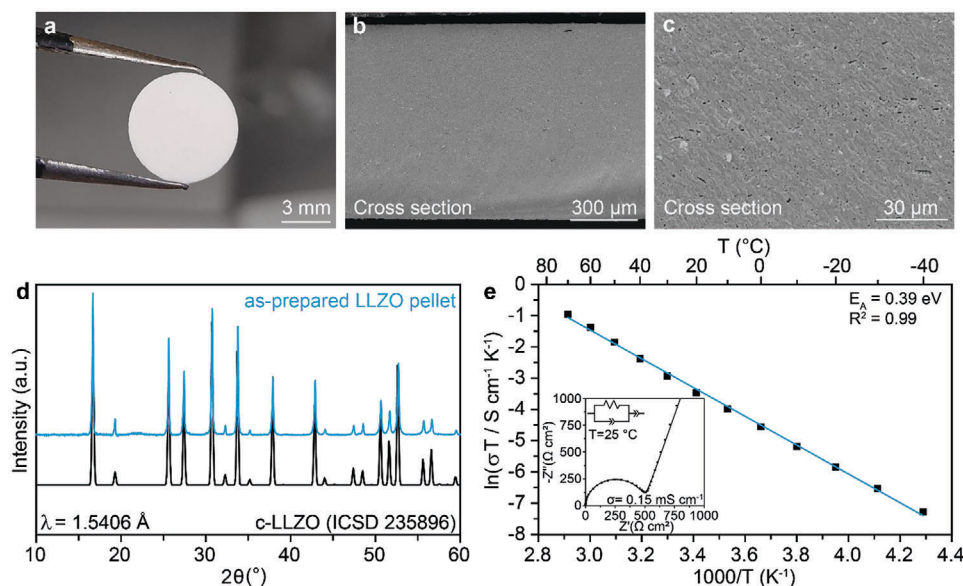


**Figure 1.** a) Photograph and b,c) cross-sectional SEM images of as-sintered LLZO pellet. d) Powder X-ray diffraction pattern of as-sintered LLZO pellet after heat-treatment at 900 °C for 10 min in Ar atmosphere. e) Arrhenius plot of as-sintered LLZO pellet [inset: impedance spectrum of Au-coated LLZO pellet at  $T = 25$  °C (dots) and fitted data (line)].

$\approx 1.5$  MPa. Stripping Li at lower pressures resulted in significant polarization of the Li/LLZO/Li symmetrical cell. It is worth noting that while many other studies have explored the impact of pressure and temperature on void formation,<sup>[20–22]</sup> they have mainly focused on the general trend of mitigated void formation with increasing pressure and temperature, rather than determining the critical stack pressure. Notably, the influence of pressure on the formation of void was also assessed computationally.<sup>[23–29]</sup>

Following the initial work of Sakamoto et al.,<sup>[19]</sup> reporting methodology for determining critical stack pressure, we sought to further investigate the phenomenon of the void formation, and aimed to underscore the significance of another factor in unveiling the critical stack pressure, which is the amount of stripped Li (the areal capacity). In contrast to the previous areal capacity limitations of 0.5, 1, and 2 mAh cm<sup>-2</sup>, our study expanded the range to 3 mAh cm<sup>-2</sup>. This expanded assessment of critical stack pressure is essential for evaluating the necessary pressure for cycling full cells that incorporate cathodes with maximized areal capacity. Furthermore, in contrast to the reported methodology of monitoring voltage polarization using a single pellet while decreasing pressure from high to low, our study explores an alternative approach to determining the critical stack pressure. We used multiple identical symmetric cells tested at different stack pressures, thus eliminating the factor of non-identical Li/LLZO interfaces formed after Li stripping at previous pressure steps, in the case of one-cell measurements. Additionally, we assessed the methodology for determining the critical temperature by conducting analogous measurements at a specific pressure of 1.25 MPa. The effectiveness of the presented approach in evaluating the suitability of temperature, pressure, and areal-capacity-limit conditions for mitigating of the void formation during Li stripping was assessed through cycling stability tests conducted on the Li/LLZO/Li symmetrical cells.

## 2. Results and Discussion

The studies on stripping/plating of Li at the Li/LLZO interface were performed using LLZO pellets prepared by ultrafast sintering of isostatically compressed commercial LLZO powders with a nominal composition of Li<sub>6.25</sub>Al<sub>0.25</sub>La<sub>3</sub>Zr<sub>2</sub>O<sub>12</sub> (Figure 1a). Ultrafast sintering was performed using a custom-made setup comprising two copper electrodes and two superimposed carbon felts clamped between the electrodes.<sup>[30]</sup> In a standard sintering experiment, the green-body LLZO pellet was positioned between two carbon foils and boron nitride plates. These layers were then inserted between two pieces of stretched carbon felts that served as heating elements (see temperature profile in Figure S1, Supporting Information). After sintering, the LLZO pellets were subjected to a heat-treatment at 600 °C under oxygen flow to remove carbon impurities originating from the graphite foil. Subsequently, an additional heat-treatment at 900 °C for 10 min in an argon environment was performed to remove Li<sub>2</sub>CO<sub>3</sub> that had formed on the LLZO surface during the prior heat-treatment.<sup>[31]</sup>

The cross-sectional scanning electron microscope (SEM) images (Figure 1b,c) demonstrate the homogeneous density of the as-prepared LLZO pellet ( $\approx 90\%$  of the theoretical density of 5.1 g cm<sup>-3</sup>). Powder X-ray diffraction (PXRD) and Raman spectroscopy measurements (Figure 1d; Figure S2, Supporting Information) confirmed the pure cubic LLZO structure after sintering and heat-treatment steps (space group Ia $\bar{3}$ d,  $a = 12.9622(2)$  Å,  $V = 2177.89$  Å<sup>3</sup>, ICSD 235 896).<sup>[32]</sup> The Li-ion conductivity and activation energy of the as-prepared LLZO pellets were estimated to be  $ca. 0.15 \pm 0.01$  mS cm<sup>-1</sup> (RT) and 0.39 eV, respectively (Figure 1e; Figures S3 and S4, Supporting Information), which are in agreement with previously reported values for LLZO pellets.<sup>[33,34]</sup>

To assess the chemical purity of the surface of as-prepared LLZO pellets, which has direct impact on the behavior of Li plating/stripping at the Li/LLZO interface, pellets were analyzed

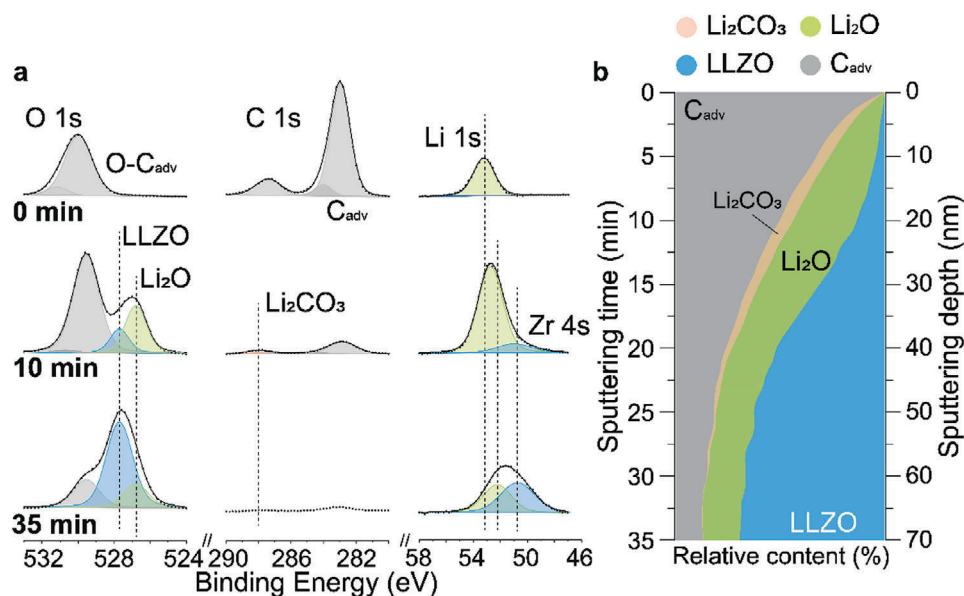


**Figure 2.** a) Charge-corrected O 1s, C 1s, Li 1s, and Zr 4s XPS spectra of as-sintered LLZO pellets after heat-treatment at 900°C for 10 min in Argon atmosphere, collected before and after sputtering (10 min, 35 min). b) Composition of the LLZO surface as a function of sputtering depth.

in depth by X-ray photoelectron spectroscopies (XPS) combined with Ar-ion sputter depth profiling. It should be noted that the XPS system was directly connected to an Ar-filled glovebox, and therefore, the fabricated samples could be transferred for the analysis without air exposure. **Figure 2** shows the measured O 1s, C 1s, Li 1s, and Zr 4s spectra of the surface of LLZO pellet and the corresponding chemical composition of the LLZO surface at different sputtering depths. XPS survey spectra of an argon heat-treated LLZO pellet, corresponding compositional sputter-depth profiles and detailed XPS spectra are shown in Figures S5–S6 (Supporting Information), respectively. As shown in Figure 2, the surface of LLZO consists mainly of adventitious carbon, as evidenced by the presence of the C 1s peaks at 282.9 eV, 284.1 eV, and 287.5 eV and the O 1s peaks at 529.5 eV and 530.7 eV, which can be unambiguously assigned to C–C, C = O, O = C–O, and O = C, O = C–O bonds, respectively.<sup>[31]</sup> The presence of adventitious carbon inevitably results from the interaction of volatile organics in the glove box with the LLZO surface. The presence of the C 1s and Li 1s lines at 288.2 eV and 53.2 eV also confirms the presence of a small amount of Li<sub>2</sub>CO<sub>3</sub> on the LLZO surface. Importantly, the La 3d, Zr 4s, and O 1s peaks originating from the LLZO lattice could only be clearly detected for sputter depths greater than 10 nm. Another O 1s peak at 526.8 eV at the sputtering depth of 10 nm through LLZO bulk can be attributed to Li<sub>2</sub>O (Li–O bonds), most likely originating from the Li<sub>2</sub>O along the rough surface of the LLZO grains and the open pores.<sup>[31,35]</sup>

Following a comprehensive characterization of the as-prepared LLZO pellets, electrochemical experiments were carried out to investigate lithium stripping at the Li/LLZO interface. These experiments were conducted under different pressure and temperature conditions, using symmetrical Li/LLZO/Li cells. Upon applying current to the symmetrical cell, thereby generating lithium stripping and plating on opposing sides of the cell, the corresponding potential response was monitored to trace the deviation from Ohmic behavior over time. This deviation primarily arises

from the formation of voids during the process of lithium stripping at specific current densities. Notably, despite the known ability of various interfacial layers between LLZO and Li to reduce the Li/LLZO interfacial resistance and mitigate void formation,<sup>[35–38]</sup> this study did not explore their influence on the critical stack pressure and temperature of the Li/LLZO interface. Our focus remained on examining Li/LLZO/Li symmetrical cells with an uncoated LLZO surface.

The Li/LLZO/Li symmetrical cells were fabricated by isostatically pressing lithium foil with a thickness of  $\approx 100 \mu\text{m}$  at a pressure of  $\approx 350 \text{ MPa}$  onto the  $700 \mu\text{m}$  – thick LLZO pellets. As follows from electrochemical impedance spectroscopy (EIS) measurements, the Li/LLZO interfacial resistance of the prepared cells was *ca.*  $115 \Omega \text{ cm}^2$  (Figure S8, Supporting Information). Galvanostatic electrochemical measurements were performed by applying a current density of  $0.2 \text{ mA cm}^{-2}$  to Li/LLZO/Li symmetrical cells and limiting areal capacity of Li stripping to  $3 \text{ mAh cm}^{-2}$ . The selection of current density was based on prior critical current density (CCD) measurements performed on identically prepared Li/LLZO/Li symmetrical cells (Figure S9, Supporting Information). As follows from CCD data, this value of the current density, on one hand, is the highest at which Li dendrite propagation does not start. On the other hand, it is sufficiently high to maximize the effect of void formation at the Li/LLZO interface. The choice of high areal capacity limit of  $3 \text{ mAh cm}^{-2}$  was driven by the stringent requirement for the areal capacity of both anodes and cathodes to maximize the energy density of Li-garnet batteries. For example, as discussed in by Sakamoto et al.,<sup>[39]</sup> to achieve an energy density greater than  $250 \text{ Wh kg}^{-1}$ , one must use electrodes with an areal capacity of at least  $2.5 \text{ mAh cm}^{-2}$ . This is the case for a cell consisting of a LiCoO<sub>2</sub> cathode infiltrated with ionic liquid or carbonate-based electrolytes and combined with a  $20\text{-}\mu\text{m}$ -thick LLZO membrane.

The resulting data, demonstrating voltage variations as a function of the areal capacity (the amount of stripped Li from

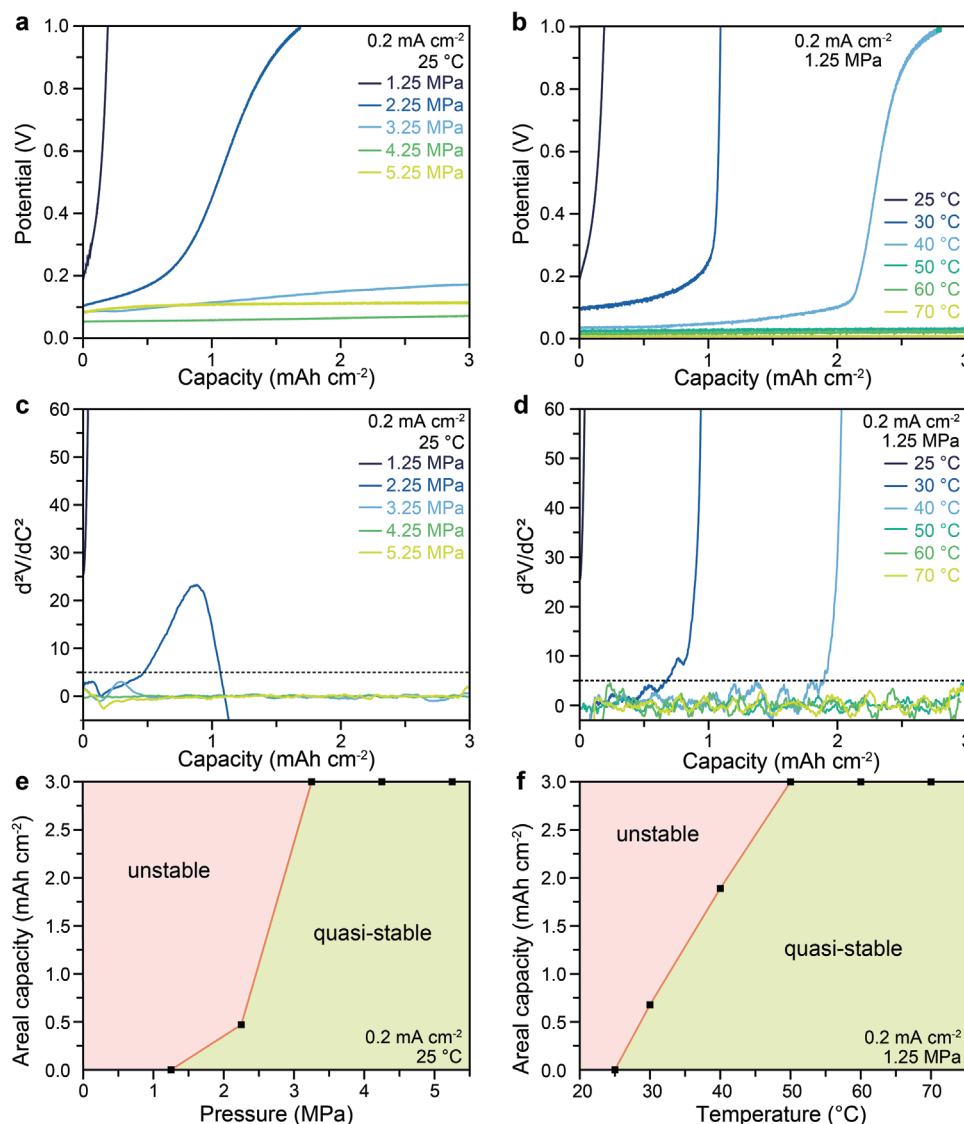


**Figure 3.** a) Voltage profiles of the Li/LLZO/Li symmetrical cells measured at different pressures (1.25–5.25 MPa) and room temperature using a current density of 0.2 mA cm<sup>-2</sup>. b) Voltage profiles of the Li/LLZO/Li symmetrical cells measured at different temperatures (25–70 °C) and a constant pressure of 1.25 MPa using a current density of 0.2 mA cm<sup>-2</sup>. c,d) Second derivatives of the curves shown in (a) and (b), respectively (V is the voltage; V is the capacity). The threshold, representing the maximum stripping areal capacity of Li in the quasi-stable stripping regime is drawn as a dashed line. e,f) Illustration of the unstable or quasi-stable Li stripping behavior from the Li/LLZO interface as a function of applied pressure e) /temperature f) and stripping areal capacity. The impedance spectra of Li/LLZO/Li symmetric cells before and after Li stripping under unstable (RT, 1.25 MPa) and quasi-stable (RT, 5.25 MPa) and (70 °C, 1.25 MPa) operating conditions can be found in the Supporting Information (Figure S10, Supporting Information). FIB-SEM cross-sectional images of the Li/LLZO interface after room temperature Li stripping at two different pressures of 1.25 MPa and 5.25 MPa are shown in Figure S11 (Supporting Information).

Li/LLZO interface) within a pressure range spanning from 1.25 to 5.25 MPa, are concisely presented in Figure 3a. An analysis of Figure 3a yields several significant conclusions. As anticipated, higher pressure levels effectively minimize voltage polarization and mitigate the formation of voids. This is evident from the significant reduction in polarization observed at elevated pressures. However, despite the application of substantial pressure, such as 5 MPa, the positive slopes observed in the curves during Li stripping indicate that the creep rate remains insufficient to entirely mitigate void formation. Consequently, the electrochemical methodology employed does not allow for a precise determi-

nation of the critical stack pressure value, but rather allows for a qualitative identification of the stack pressure required to achieve quasi-stable Li stripping regime with minimal void formation. In contrast, the second derivative of the voltage profile can be employed as an indicator of quasi-stable or unstable conditions during Li stripping. When the second derivative deviates from zero, indicating a nonlinear increase in overpotential, it signals unstable Li stripping conditions, suggesting a rapid change in the rate of void formation. Conversely, if the second derivative remains close to zero, it points to a quasi-stable Li stripping regime in which the interface can be considered quasi-stable. Therefore, in

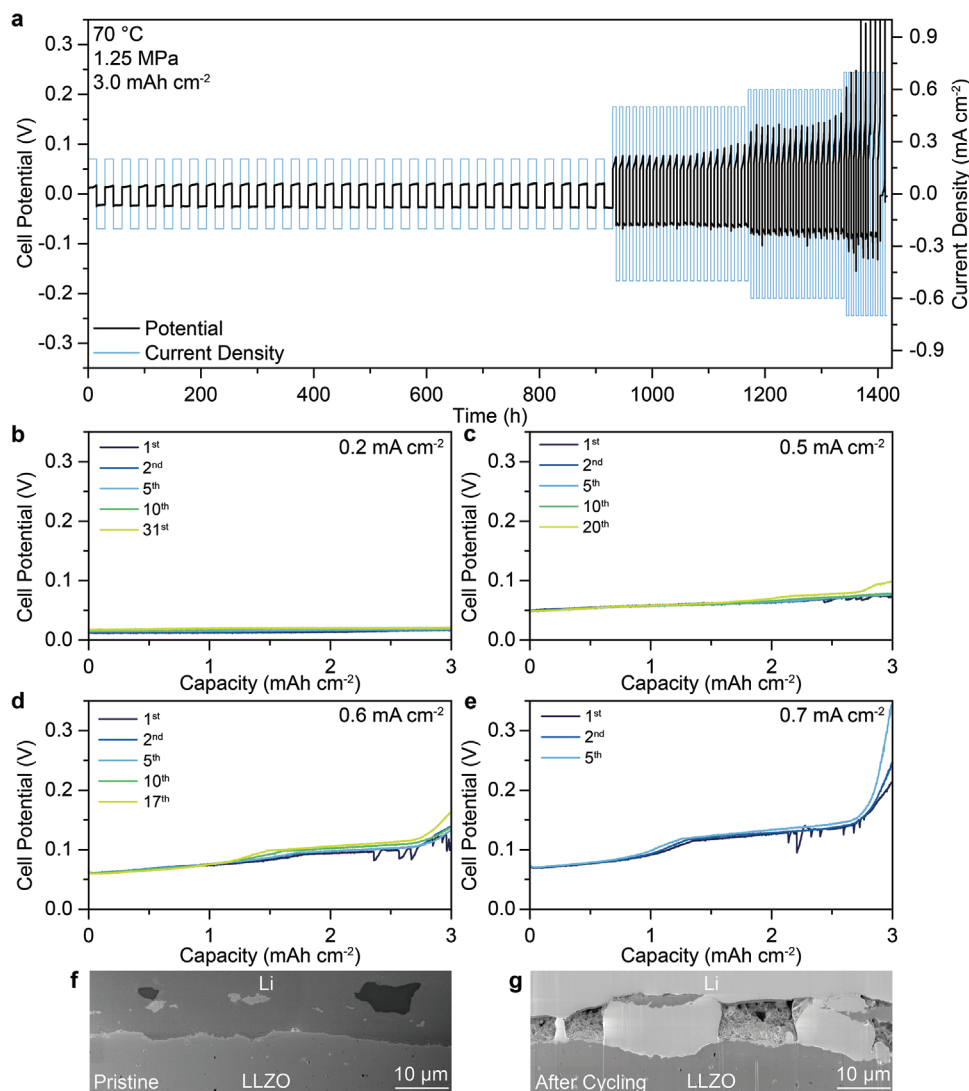


**Figure 4.** a) Voltage profiles of the Li/LLZO/Li symmetrical cell, measured at current densities of 0.2, 0.5, 0.6, and 0.7 mA cm<sup>-2</sup>, with a capacity limitation of 3 mAh cm<sup>-2</sup> per half-cycle. Measurements were performed at a pressure of 1.25 MPa and a temperature of 70 °C. Enlarged individual voltage profiles, measured at a current densities of 0.2 b), 0.5 c), 0.6 d), and 0.7 mA cm<sup>-2</sup> e). Cross-sectional FIB-SEM images of the Li/LLZO interface of the Li/LLZO/Li symmetrical cell before f) and after g) cycling.

the context of the experimental approach employed, we propose to use of the term “quasi-stable critical stack pressure” instead of “critical stack pressure”, which represents the boundary between unstable and quasi-stable Li stripping conditions. Notably, the concept of using the second derivative as an indicator of an unstable/quasi-stable regime was first introduced by Sakamoto et al.<sup>[22]</sup> when studying the effect of Li thickness on the electrochemical performance of Li/LLZO anodes. Importantly, analysis of the second derivatives of the voltage profiles recorded at different pressures indicates that a pressure of 3.25 MPa or higher is required to achieve quasi-stable Li stripping behavior (Figure 3c). In contrast, utilizing pressures of 1.25 and 2.25 MPa fails to stabilize the Li/LLZO interface during Li stripping, ultimately resulting in a nonlinear increase in voltage polarization. A more visually intuitive representation of the data in Figure 3c is provided in Figure 3e. This figure illustrates the range of pressure

values and the corresponding maximum Li stripping area capacity at which unstable or quasi-stable Li stripping conditions can be anticipated at a current density of 0.2 mA cm<sup>-2</sup>. Next, to comprehend the impact of the temperature on achieving the quasi-stable Li-stripping conditions, we performed additional measurements of the symmetrical Li/LLZO/Li cells at different temperatures while maintaining a constant pressure of 1.25 MPa. The results of these experiments are consolidated in Figure 3b,d,f.

Notably, the temperature plays a crucial role in reducing the voltage polarization, as evidenced by the significantly flatter slopes of the voltage profiles compared to those observed at room temperature, even at higher pressures in the range of 3–5 MPa. Furthermore, these findings reveal that even a relatively low temperature of 50 °C enables the stabilization of the Li/LLZO interface, even when applying the minimum pressure of 1.25 MPa (Figure 3d,f). These results align with the observations made by

Hatzell et al.,<sup>[20]</sup> highlighting the substantial impact of temperature in mitigating void formation. It should also be noted that the observed quasi-stable lithium stripping conditions, i.e., a temperature of 50°C and a stack pressure of 1.25 MPa, are within the requirements for practical application in electric vehicles.<sup>[40,41]</sup>

To validate the robustness of our methodology for identifying unstable and quasi-stable Li-stripping conditions and, consequently, to assess the effectiveness of the selected pressure, temperature, and areal capacity limit in achieving high cycling performance for a Li anode in conjunction with an LLZO solid-state electrolyte, we conducted cycling stability tests on the symmetrical Li/LLZO/Li cells. These experiments were performed under quasi-stable conditions, involving a pressure of 1.25 MPa, a temperature of 70°C and areal capacity limit of 3 mAh cm<sup>-2</sup>. Notably, the voltage profiles obtained from the Li/LLZO/Li symmetrical cell at a current density of 0.2 mA cm<sup>-2</sup> remained relatively stable for ≈30 cycles (Figure 4a,b). These results indicate that under the applied conditions, it is indeed possible to effectively mitigate void formation and underscores the practical utility of the discussed methodology in determining the quasi-critical stack pressure or temperature. It is important to note, however, that these maps are applicable when maintaining the same current density, which in our case was 0.2 mA cm<sup>-2</sup>. If the current density is increased, the pressure-temperature conditions must be adjusted accordingly. This is demonstrated in Figure 4c–e, which show voltage profiles at higher current densities of 0.5, 0.6, and 0.7 mA cm<sup>-2</sup>, revealing increased voltage polarization and indicating the presence of void formation. This observation was further confirmed by focused-ion-beam scanning electron microscopy (FIB-SEM) measurements, which unveiled the formation of 10-μm sized voids at the Li/LLZO interface after cycling the Li/LLZO/Li symmetrical cell at the current density of 0.7 mA cm<sup>-2</sup> (Figure 4f,g).

### 3. Conclusions

In summary, our research has focused on understanding the role of stack pressure and temperature in mitigating the well-known issue of void formation at the Li/LLZO interface during high-current-density Li stripping. We have examined the methodology for assessing the quasi-critical stack pressure and temperature of Li metal anodes when paired with LLZO solid-state electrolytes. It is based on the comparative analysis of the voltage profiles and their second derivatives obtained from galvanostatic measurements over the one half-cycle, employing identical Li/LLZO/Li symmetrical cells at varying pressures. In particular, we have demonstrated that the second derivative of the voltage profile can be used as an indicator of the stability of the Li/LLZO interface during Li stripping, thereby enabling the determination of the ranges of pressure, temperature, and maximum achievable areal capacity of Li stripping at which the impact of the void formation can be minimized. For instance, our experiments have unveiled that quasi-stable Li stripping in Li/LLZO/Li symmetrical cells at a current density of 0.2 mA cm<sup>-2</sup> can be achieved at a 3.25 MPa at room temperature or 1.25 MPa at 50°C. Importantly, we demonstrated the effectiveness of this methodology by conducting cycle stability tests (current density of 0.2 mA cm<sup>-2</sup> and areal capacity limit of 3 mAh cm<sup>-2</sup>) on the Li/LLZO/Li symmet-

rical cells in combination with Li/LLZO cross-sectional FIB-SEM measurements.

### 4. Experimental Section

**Preparation of LLZO Pellets:** 240 mg of aluminum-doped LLZO (Al-LLZO powder, Ampcera, 500 nm nanopowder) was loaded into a die ( $d = 1$  cm) and uniaxially compressed with a force of ≈10 kN. The surface of the green body pellets was then carefully polished with SiC abrasive paper to remove any visible impurities. The polished pellets were dried in air at 200°C for 30 min, followed by additional heat-treatment at 900°C for 10 min in an argon-filled glove box (Inert Corp, O<sub>2</sub> < 0.1 ppm, H<sub>2</sub>O < 0.5 ppm) on the sacrificial LLZO pellets as a substrate. Sintering of the as-prepared LLZO pellets was performed using a custom setup (see Ref. [30]) under an argon atmosphere (in an Ar-filled glove box) between two graphite foils. The pellets were pre-heated to 1000°C for 20 s and then sintered at 1200°C for 120 s (see Figure S1, Supporting Information for a typical temperature profile). To remove any carbon impurities from the surface, the sintered pellets were then heat-treated at 600°C for 2 h (heating rate: 600°C h<sup>-1</sup>) in an oxygen atmosphere and polished with 20-μm diamond paper to a thickness of ≈700 μm. For a final surface treatment, the pellets were placed in the Ar-filled glove box and heat-treated at 900°C for 10 min on the sacrificial LLZO pellets as a substrate.

**Symmetrical Cell Preparation:** Symmetrical cells were fabricated by isostatic pressing lithium metal discs (thickness ≈ 100 μm and  $d \approx 6$  mm) to on both sides of an Al-LLZO pellet at a pressure of 1000 kN (equivalent to ≈350 MPa) using a PW 100 EH cold isostatic press (P/P/Weber) for 3 min in an inert environment. Lithium metal discs were prepared from the small pieces of lithium metal rod by rolling them into a foil.

**Electrochemical Testing:** Electrochemical measurements of Li/LLZO/Li symmetrical cells under pressure and the temperature were performed in the argon-filled glovebox, using the custom-made setup (Figure S12, Supporting Information) connected to a BioLogic VMP-300 multichannel workstation. Electrochemical impedance spectroscopy measurements were conducted with a BioLogic SAS MTZ-35 using a frequency range of 35 MHz to 10 Hz with a sinus peak amplitude of 10 mV.

**Materials Characterization:** PXRD was measured on a STOE STADI P powder X-ray diffractometer in transmission mode (Cu-K<sub>α1</sub> irradiation,  $\lambda = 1.5406$  Å). Fracture cross-section SEM images were recorded on a Hitachi TM3030Plus tabletop microscope with an acceleration voltage of 5 kV. Cross-section FIB-SEM images were prepared on a Thermo Fisher Scientific Helios 5 Hydra Multi-Ion-Species Plasma FIB Microscope. Cross-sections were made by argon ion beam milling with an acceleration voltage of 30 kV and a current of up to 2.0 μA. Corresponding SEM images were recorded with a stage tilt of 52° using an acceleration voltage of 2 kV in secondary electron mode. The images are shown with tilt correction.

XPS analysis was performed using a PHI Quantes spectrometer (ULVAC-PHI), equipped with a conventional low-energy Al-K<sub>α</sub> source (1486.6 eV). The XPS spectrometer was directly connected to an Ar-filled glove box, thus allowing an *in-situ* transfer of LLZO pellets between the synthesis and XPS glovebox without their exposure to air. The energy scale of the hemispherical analyzer was calibrated according to ISO 15 472 by referencing the Au 4f7/2 and Cu 2p3/2 main peaks (as measured *in situ* for corresponding sputter-cleaned, high-purity metal references) to the recommended BE positions of 83.96 eV and 932.62 eV, respectively. The probing depths for the La 3d, Zr 3d, O 1s, C 1s, and Li 1s spectra recorded from LLZO using Al-K<sub>α</sub> X-ray radiation ( $h\nu = 1486.7$  eV) are 3.6, 5.5, 4.8, 5.5, and 6.6 nm, respectively.<sup>[35]</sup> Charge neutralization during each measurement cycle was performed with a dual beam charge neutralization system using low-energy electron and argon-ion beams (1 V bias, 20 μA current).

Compositional sputter-depth profiles were obtained by performing alternating cycles of XPS measurement (Al-K<sub>α</sub> at 51 W; beam diameter ≈200 μm) and sputtering with a focused 1 keV Ar beam, rastering an area of 2×2 mm<sup>2</sup>. During each measurement cycle, the Li 1s, La 3d, Zr 3d, C 1s, and O 1s regions were recorded with a step size of 0.05 eV and

a pass energy of 280 eV. The etch rate was calibrated to be  $2 \text{ nm min}^{-1}$  on a 100 nm  $\text{Ta}_2\text{O}_5/\text{Ta}$  reference sample. XPS survey spectra, covering the binding energy (BE) range of 0 eV – 1200 eV (XPS), were recorded with a step size of 0.5 eV at a constant pass energy of 280 eV using the Al-K $\alpha$  source (power 51 W; beam diameter  $\approx 200 \mu\text{m}$ ). Importantly, considering that the same binding energy position (282.9 eV) of C-C peaks was observed in each spectrum at different sputtering depths due to constant charging effect on the LLZO sample,<sup>[42]</sup> their calibration was not performed. For comparison with literature data, all peak positions of spectra can be shifted forward by 1.9 eV to higher binding energies.

Spectral reconstruction was performed by linear-least squares fitting of the background corrected spectra with one or more symmetric, mixed Gaussian–Lorentzian line shape functions using the CasaXPS software. The Gaussian fraction of each peak component (representative of instrumental broadening) was constrained to 0.5. The same full width at half maximum (FWHM) and relative BE position of each peak component were kept constant when fitting peaks at different sputtering depths. Notably, the peak shape and position of Li 1s at each depth were set to free, as it is impossible to differentiate between the different Li 1s chemical species (the chemical shifts are too small as compared to the intrinsic line width). The quantitative analysis of each component shown in Figure S6 (Supporting Information) was performed by calculating the areas of the fitted peaks without normalization. The relative composition profiles of  $\text{Li}_2\text{O}$  and LLZO were estimated from the quantitative analysis of the O 1s spectrum with a relative sensitivity factor of 2.93, while the relative compositions of  $\text{Li}_2\text{CO}_3$  and  $\text{C}_{\text{adv}}$  were estimated from the C 1s spectrum with a relative sensitivity factor of 1.

Raman spectroscopy measurements were conducted on a Horiba LabRAM HR Evolution UV-VIS-NIR system using a 532 nm laser with a power of 300 mW. The samples were sealed between thin glass slides in an Argon atmosphere.

## Supporting Information

Supporting Information is available from the Wiley Online Library or from the author.

## Acknowledgements

The authors are grateful to the research facilities of ETH Zurich (Scientific Center for Optical and Electron Microscopy and Small Molecule Crystallography Center, Department of Chemistry and Applied Biosciences) and Empa (Laboratory for Mechanics of Materials & Nanostructures) for access to the instruments and for technical assistance. The authors gratefully acknowledge the funding from the Innosuisse (grant No. 58207.1). The authors thank Dr. Claudia Cancellieri for her assistance in XPS measurements, and Dr. Joakim Reuteler and Dr. Sung-Sik Lee from ScopeM for their support and assistance in conducting measurements on the Thermo Fisher Scientific Helios 5 Hydra system and the Horiba Raman microscope, respectively.

## Conflict of Interest

The authors declare no conflict of interest.

## Data Availability Statement

The data that support the findings of this study are available from the corresponding author upon reasonable request.

## Keywords

critical stack pressure, Li metal anode, LLZO solid-state electrolyte, solid-state batteries, void formation

Received: November 8, 2023

Revised: December 13, 2023

Published online:

- [1] J. Janek, W. G. Zeier, *Nat. Energy* **2016**, *1*, 16141.
- [2] Z. Zhang, Y. Shao, B. Lotsch, Y.-S. Hu, H. Li, J. Janek, L. F. Nazar, C.-W. Nan, J. Maier, M. Armand, L. Chen, *Energy Environ. Sci.* **2018**, *11*, 1945.
- [3] V. Thangadurai, S. Narayanan, D. Pinzaru, *Chem. Soc. Rev.* **2014**, *43*, 4714.
- [4] K. V. Kravchik, D. T. Karabay, M. V. Kovalenko, *Sci. Rep.* **2022**, *12*, 1177.
- [5] K. J. Kim, M. Balaish, M. Wadaguchi, L. Kong, J. L. M. Rupp, *Adv. Energy Mater.* **2021**, *11*, 2002689.
- [6] X.-B. Cheng, R. Zhang, C.-Z. Zhao, Q. Zhang, *Chem. Rev.* **2017**, *117*, 10403.
- [7] E. Rangasamy, J. Wolfenstine, J. Sakamoto, *Solid State Ion.* **2012**, *206*, 28.
- [8] J. Košir, S. Mousavihashemi, B. P. Wilson, E.-L. Rautama, T. Kallio, *Solid State Ion.* **2022**, *380*, 115943.
- [9] Q. Zhao, S. Stalin, C.-Z. Zhao, L. A. Archer, *Nat. Rev. Mater.* **2020**, *5*, 229.
- [10] J. G. Connell, T. Fuchs, H. Hartmann, T. Krauskopf, Y. Zhu, J. Sann, R. Garcia-Mendez, J. Sakamoto, S. Tepavcevic, J. Janek, *Chem. Mater.* **2020**, *32*, 10207.
- [11] Y. Zhu, J. G. Connell, S. Tepavcevic, P. Zapol, R. Garcia-Mendez, N. J. Taylor, J. Sakamoto, B. J. Ingram, L. A. Curtiss, J. W. Freeland, D. D. Fong, N. M. Markovic, *Adv. Energy Mater.* **2019**, *9*, 1803440.
- [12] H. Sun, S. Kang, L. Cui, *J. Chem. Eng.* **2023**, *454*, 140375.
- [13] J. Janek, W. G. Zeier, *Nat. Energy* **2023**, *8*, 230.
- [14] S. Randau, D. A. Weber, O. Kötz, R. Koerver, P. Braun, A. Weber, E. Ivers-Tiffée, T. Adermann, J. Kulisch, W. G. Zeier, F. H. Richter, J. Janek, *Nat. Energy* **2020**, *5*, 259.
- [15] H. Koshikawa, S. Matsuda, K. Kamiya, M. Miyayama, Y. Kubo, K. Uosaki, K. Hashimoto, S. Nakanishi, *J. Power Sources* **2018**, *376*, 147.
- [16] T. Krauskopf, H. Hartmann, W. G. Zeier, J. Janek, *ACS Appl. Mater. Interfaces* **2019**, *11*, 14463.
- [17] M. Klimpel, H. Zhang, M. V. Kovalenko, K. V. Kravchik, *Commun. Chem.* **2023**, *6*, 192.
- [18] K. V. Kravchik, H. Zhang, F. Okur, M. V. Kovalenko, *Acc. Mater. Res.* **2022**, *3*, 411.
- [19] M. J. Wang, R. Choudhury, J. Sakamoto, *Joule* **2019**, *3*, 2165.
- [20] W. Zaman, L. Zhao, T. Martin, X. Zhang, Z. Wang, Q. J. Wang, S. Harris, K. B. Hatzell, *ACS Appl. Mater. Interfaces* **2023**, *15*, 37401.
- [21] S. Matsuda, K. Nakamura, *ACS Appl. Energy Mater.* **2020**, *3*, 11113.
- [22] K. Lee, E. Kazyak, M. J. Wang, N. P. Dasgupta, J. Sakamoto, *Joule* **2022**, *6*, 2547.
- [23] M. Feng, C.-T. Yang, Y. Qi, *J. Electrochem. Soc.* **2022**, *169*, 090526.
- [24] X. Zhang, Q. J. Wang, K. L. Harrison, S. A. Roberts, S. J. Harris, *Cell Rep. Phys. Sci.* **2020**, *1*, 100012.
- [25] X. Zhang, Q. J. Wang, K. L. Harrison, K. Jungjohann, B. L. Boyce, S. A. Roberts, P. M. Attia, S. J. Harris, *J. Electrochem. Soc.* **2019**, *166*, A3639.
- [26] H. Yan, K. Tantratian, K. Ellwood, E. T. Harrison, M. Nichols, X. Cui, L. Chen, *Adv. Energy Mater.* **2022**, *12*, 2102283.
- [27] B. S. Vishnugopi, K. G. Naik, H. Kawakami, N. Ikeda, Y. Mizuno, R. Iwamura, T. Kotaka, K. Aotani, Y. Tabuchi, P. P. Mukherjee, *Adv. Energy Mater.* **2023**, *13*, 2203671.
- [28] R. Raj, *Acta Mater.* **2021**, *215*, 117076.
- [29] J. A. B. Agier, S. S. Shishvan, N. A. Fleck, V. S. Deshpande, *Acta Mater.* **2022**, *240*, 118303.

- [30] H. Zhang, R. Dubey, M. Inniger, F. Okur, R. Wullich, A. Parrilli, D. T. Karabay, A. Neels, K. V. Kravchyk, M. V. Kovalenko, *Cell Rep. Phys. Sci.* **2023**, 4, 101473.
- [31] H. Zhang, G. Paggiaro, F. Okur, J. Huwiler, C. Cancellieri, L. P. H. Jeurgens, D. Chernyshov, W. Van Beek, M. V. Kovalenko, K. V. Kravchyk, *ACS Appl. Energy Mater.* **2023**, 6, 6972.
- [32] C. Hiebl, D. Young, R. Wagner, H. M. R. Wilkening, G. J. Redhammer, D. Rettenwander, *J. Phys. Chem. C* **2019**, 123, 1094.
- [33] N. J. Taylor, S. Stangeland-Molo, C. G. Haslam, A. Sharafi, T. Thompson, M. Wang, R. Garcia-Mendez, J. Sakamoto, *J. Power Sources* **2018**, 396, 314.
- [34] S. Afyon, K. V. Kravchyk, S. Wang, J. V. D. Broek, C. Hänsel, M. V. Kovalenko, J. L. M. Rupp, *J. Mater. Chem. A* **2019**, 7, 21299.
- [35] R. Dubey, J. Sastre, C. Cancellieri, F. Okur, A. Forster, L. Pompizii, A. Priebe, Y. E. Romanyuk, L. P. H. Jeurgens, M. V. Kovalenko, K. V. Kravchyk, *Adv. Energy Mater.* **2021**, 11, 2102086.
- [36] W. Luo, Y. Gong, Y. Zhu, K. K. Fu, J. Dai, S. D. Lacey, C. Wang, B. Liu, X. Han, Y. Mo, E. D. Wachsman, L. Hu, *J. Am. Chem. Soc.* **2016**, 138, 12258.
- [37] Y. Fan, T. Tao, Y. Gao, C. Deng, B. Yu, Y. I. Chen, S. Lu, S. Huang, *Adv. Mater.* **2020**, 32, 2004798.
- [38] D. Kim, Y. Fan, S. Mateti, Y. Chen, X. Hu, Q. Cai, B. Yu, Y. I. Chen, *Nano Energy* **2023**, 117, 108890.
- [39] K. V. Kravchyk, F. Okur, M. V. Kovalenko, *ACS Energy Lett.* **2021**, 6, 2202.
- [40] M. J. Wang, E. Kazyak, N. P. Dasgupta, J. Sakamoto, *Joule* **2021**, 5, 1371.
- [41] W. Zaman, K. B. Hatzell, *Curr. Opin. Solid State Mater. Sci.* **2022**, 26, 101003.
- [42] H. Zhang, F. Okur, C. Cancellieri, L. P. H. Jeurgens, A. Parrilli, D. T. Karabay, M. Nesvadba, S. Hwang, A. Neels, M. V. Kovalenko, K. V. Kravchyk, *Adv. Sci.* **2023**, 10, 2205821.